CYCLIC AND OPTIMAL CLUSTER FLIGHT OF MULTIPLE SATELLITES USING DIFFERENTIAL DRAG

Ohad Ben-Yaacov [(1)]**, and Pini Gurfil** [(2)]
[(1)] *Graduate Student, Faculty of Aerospace Engineering, Technion - Israel Institute of Technology, Haifa 32000, Israel, +972-4-8293512, ohadby@technion.ac.il*
[(2)] *Associate Professor, Faculty of Aerospace Engineering, Technion - Israel Institute of Technology, Haifa 32000, Israel, +972-4-8294973, pgurfil@technion.ac.il*

Abstract: *The idea to use differential drag (DD) for satellite formationkeeping emerged in the mid-Eighties, when the feasibility of DD-based control was proven assuming linearized relative dynamics for two satellites. Unlike previous work in differential drag-based formationkeeping, the present work develops a nonlinear method suitable for missions in excess of a year. It is first shown that the differential mean eccentricity in uncontrollable for near-circular orbits, and hence a nonlinear DD-based controller for matching the drag-related secular component of the semimajor axis is developed. An asymptotic stability proof for the controller is provided. Moreover, two new methods for DD-based cluster-keeping of multiple modules are developed, thus expanding existing literature, which usually deals with two satellites only. The results are validated using simulations based on the forthcoming Space Autonomous Mission for Swarming and Geolocation with Nanosatellites, showing that DD-based cluster-keeping can be effective for altitudes reaching about 600 km.*

Keywords: *Disaggregated satellites, cluster flight, cluster-keeping*

1. Introduction

One of the emerging concepts in future space technologies is that of disaggregated satellites. The idea is to distribute a single satellite into multiple free-flying modules, without changing the functionality of the whole system. The modules are physically independent, interacting through a wireless network. One of the key issues in disaggregated spacecraft is the relative position control, known as cluster flight. As opposed to a single satellite or conventional formation flying satellites, there could be modules without active control capabilities (i.e. thrusters). For those modules, passive control is the only way to change the relative position in the cluster in the presence of perturbations.
For low Earth orbit (LEO) satellites, the main perturbations are the Earth oblateness and atmospheric drag. In general, the effects of perturbations on each satellite are not identical. Therefore, a relative translational drift between the satellites is inevitable. Each of the aforementioned perturbation forces induces different changes in the orbital elements (in-plane and out-of-plane relative drift). Hence, corrections are needed to keep the modules in the desired cluster.
Active control of relative satellite translation has been a popular field of study: A methodology for impulsive corrections of mean orbital element differences to mitigate the effect of J_2 perturbations was proposed by Ref. [1]; a similar rationale was adopted by Refs. [2–5], wherein periodic impulsive velocity corrections were developed. Other works developed algorithms for multi-impulsive guidance maneuvers [6], proposed two-

impulse maneuver schemes for formation reconfiguration using a two-body setup [7], and offered continuous-thrust feedback methods [8, 9].

The idea to use passive means – instead, or in addition to, thrust – to control the satellite relative orbits, was first suggested by Ref. [10], which showed that differential drag (DD) can be potentially used for formationkeeping. The analysis was based on the controlled version of the CW equations. A similar model was used in a number of subsequent works. Reference [10] used the linear equations of relative motion, and suggested utilizing the DD force by using drag plates attached to each satellite. A transformation was then performed in order to reduce the formationkeeping problem into a double integrator. Ref. [11] used again the linear equations of motion and developed an eccentricity-minimizing control scheme in order to control the formation by using DD.

Decades after the original idea, the most prevalent approach for DD-based formation-keeping still utilizes linearized LVLH models. Some of the recent efforts in this field include Refs. [12, 13], which investigated the use of linear quadratic controllers for DD based formationkeeping and Ref. [14], which suggested a bang-bang type DD controller. The same basic models have also been used in the study of DD-based rendezvous [15, 16].

Consequently, there is abundant literature on DD-based formationkeeping, but there are hardly any works on long-term cluster-keeping based on DD – let alone cluster-keeping of multiple (i.e., more than two) satellites. Using linearized LVLH models for developing DD-based formationkeeping is valid for short time periods and small relative distances. In practical situations, the effect of long-term and secular perturbations cannot be modeled using CW-type equations, since the differential forces would increase relative distances and the orbital perturbations would accumulate beyond the validity of the linearized approximation. Instead, orbital-elements based models can be utilized. In particular, cluster flight of disaggregated satellite modules is inherently a long-term mission, which must utilize astrodynamical tools suitable for long-term modeling. Moreover, most exiting works discuss the case of only two satellites, whereas there are multiple modules in a typical disaggregated space system.

The goal of the current work is to develop DD-based cluster-keeping algorithms suitable for implementation in long-term missions, with a particular emphasis on multiple modules. The underlying modeling approach utilizes orbital elements. Some previously unanswered questions are addressed: Which of the differential mean orbital elements is controllable using DD in near-circular orbits? How can an effective orbital elements feedback be constructed so as to utilize the long-term DD effect? How to use DD-based cluster-keeping if there are more than two satellites in the cluster? When would it be wise to commence a DD-based cluster-flight maneuver?

2. Background

2.1. Coordinate Systems

The subsequent analysis uses two coordinate systems:

1. I : An Earth-Centered Inertial (ECI) coordinate system. The fundamental plane is the equator, the $\hat{\mathbf{x}}$-axis is directed from the Earth's center to the vernal equinox,

the $\hat{\mathbf{z}}$-axis is normal to the fundamental plane, positive in the direction of the polar axis, and the $\hat{\mathbf{y}}$-axis completes the right-hand setup.

2. $\mathfrak{L}$: A local-vertical local-horizontal (LVLH) coordinate system, centered at the satellite. The $\hat{\mathbf{x}}$-axis is directed radially outward. The $\hat{\mathbf{z}}$-axis points in the direction of instantaneous angular momentum vector of the orbit, and the $\hat{\mathbf{y}}$-axis completes the right-hand setup.

2.2. Gauss Variational Equations

The general nonlinear dynamics of a satellite under any perturbation and/or control input can be modeled using the Gauss Variational Equations (GVEs). The GVEs are commonly written as [17]:

$$\begin{aligned}
\frac{da}{dt} &= \frac{2}{h}a^2 e(\sin f)d_r + 2\frac{a^2 p}{hr}d_\theta \\
\frac{de}{dt} &= \frac{1}{h}p(\sin f)d_r + \frac{(p+r)\cos f + re}{h}d_\theta \\
\frac{di}{dt} &= \frac{r\cos(f+\omega)}{h}d_h \\
\frac{d\Omega}{dt} &= \frac{r\sin(f+\omega)}{h\sin i}d_h \\
\frac{d\omega}{dt} &= -\frac{p\cos f}{he}d_r + \frac{(p+r)\sin f}{he}d_\theta - \frac{r\sin(f+\omega)\cos i}{h\sin i}d_h \\
\frac{dM}{dt} &= n + \frac{(-2e+\cos f + e\cos^2 f)(1-e^2)}{ena(1+e\cos f)}d_r + \frac{(e^2-1)(e\cos f+2)\sin f}{ena(1+e\cos f)}d_\theta
\end{aligned} \tag{1}$$

where a is the semimajor axis, e is the eccentricity, i denotes the inclination, Ω denotes the right ascension of the ascending node (RAAN), ω is the argument of perigee and M is the mean anomaly. In addition, $p = a(1-e^2)$, $h = \sqrt{\mu p}$, μ is the gravitational constant, $n = \sqrt{\mu / a^3}$ is the mean motion, and f is the true anomaly. The vector $\mathbf{d} = [\mathrm{d_r}, \mathrm{d}_\theta, \mathrm{d_h}]^{\mathrm{T}}$ represents perturbation or control accelerations written in $\mathfrak{L}$, where $\mathrm{d_r}$, d_θ and $\mathrm{d_h}$ are the radial, along-track, and cross-track exogenous accelerations, respectively.

2.3. Gravitational Potential

The gravitational potential includes the zonal, sectorial and tesseral harmonics. The most significant perturbations affecting the inter-satellite distance are the even zonal harmonics, because of their secular effects. The potential per unit mass of the zonal harmonics in the ECI reference frame is given by [18]:

$$\Phi(\mathbf{r}) = -\frac{\mu}{r}\left[1 - \sum_{n=2}^{\infty} J_n \left(\frac{R_e}{r}\right)^n P_n\left(\frac{z}{r}\right)\right] \tag{2}$$

where $r \triangleq \|\mathbf{r}\|$, $\mathrm{P_n}$ are Legendre polynomials of order n, $\mathrm{J_n}$ are the zonal harmonics coefficients, and $\mathrm{R_e}$ denotes the equatorial radius of the Earth.

2.4. Atmospheric Drag

The specific force due to atmospheric drag can be modeled in the ECI frame as [18]:

$$\mathbf{d}_{drag}^{ECI} = -\frac{1}{2}\rho \, \|\mathbf{v} - \mathbf{v}_{atm}\|(\mathbf{v} - \mathbf{v}_{atm})\frac{SC_D}{m} \tag{3}$$

where ρ is atmospheric density, S is the cross-sectional area normal to the satellite-atmosphere relative velocity, $\mathrm{C_D}$ is the drag coefficient, and m is the mass. The vector $\mathbf{v}$ is the velocity in ECI coordinates, and the vector $\mathbf{v}_{\mathrm{atm}}$ is the atmospheric velocity in the same frame. If the atmosphere is modeled as a rigid body, then $\mathbf{v}_{\mathrm{atm}} = \boldsymbol{\Omega}_E \times \mathbf{r}$, where $\boldsymbol{\Omega}_E$ is the spin rate of the Earth around its polar axis, written in the ECI frame.

A common approach for modeling the drag force is to neglect the atmospheric velocity. According to this assumption, the drag force acts in the orbital plane. Hence, it will affect only the elements a, e, ω and f. If an averaging procedure is used, it can be shown [18] that only the mean a and e are affected by the drag force. The averaging operator yields the mean orbital elements according to

$$\overline{\alpha} \triangleq \frac{1}{2\pi}\int_0^{2\pi} \alpha \, dM \tag{4}$$

where α denotes any orbital element and $\overline{\alpha}$ is the corresponding mean element. If the atmospheric rotational velocity is neglected and an exponential model for the density is used, the following expressions are obtained for the mean semimajor axis and eccentricity, respectively, assuming that e < 0.2 [18, 19]:

$$\dot{\bar{a}} = -2\bar{a}^2 C_B \bar{n} \rho_0 \exp\left(-\bar{\nu}\right) \sum_{k=0}^{\infty} A_k I_k\left(\bar{\nu}\right)$$
$$\dot{\bar{e}} = -2 C_B \rho_0 \overline{np} \exp\left(-\bar{\nu}\right) \sum_{k=0}^{\infty} B_k I_k\left(\bar{\nu}\right) \tag{5}$$

where $C_B \triangleq SC_D/(2m)$ is the ballistic coefficient, $\bar{n}$ is the averaged mean motion, ρ_0 is the reference density for the exponential model, $\bar{\nu} \triangleq \overline{ae}/H$, H is the atmospheric scale factor, A_K and B_K are coefficients that depend, in general, on $\bar{e}$ and $\bar{\nu}$, and I_k is the modified Bessel function of the first kind of order k:

$$I_k\left(\nu\right) \triangleq \frac{1}{\pi}\int_0^{\pi} \exp\left(\nu\cos E\right)\cos\left(kE\right)dE \tag{6}$$

Finally, let $\left(\cdot\right)_{\mathrm{D}}$ denote quantities related to a deputy module, and $\left(\cdot\right)_{\mathrm{C}}$ denote quantities associated with the chief module.

3. Orbital Elements-Based Cluster-keeping with Differential Drag

3.1. Controllability Analysis

To investigate controllability, the linear variations of the deputy's mean semimajor axis and eccentricity are examined with respect to the mean elements of the chief, based on Eq.(5):

$$\begin{bmatrix} \Delta\dot{\bar{a}} \\ \Delta\dot{\bar{e}} \end{bmatrix} = \begin{bmatrix} F_{11} & F_{12} \\ F_{21} & F_{22} \end{bmatrix} \begin{bmatrix} \Delta\bar{a} \\ \Delta\bar{e} \end{bmatrix} + \begin{bmatrix} C_1 \\ C_2 \end{bmatrix} \Delta S \tag{7}$$

where $\Delta a = a_{\mathcal{D}} - a_{\mathcal{C}}$, $\Delta e = e_D - e_C$, and $\Delta S = S_{\mathcal{D}} - S_{\mathcal{C}}$. If an expansion up to $\mathcal{O}\left(e^2\right)$ is used, then the coefficients appearing in Eq. (5) are given by:

$$A_0 = 1+\frac{3}{4}\overline{e}^2, A_1 = 2\overline{e}, A_2 = \frac{3}{4}\overline{e}^2, B_0 = \frac{\overline{e}}{2}, B_1 = 1+\frac{3}{8}\overline{e}^2, B_2 = \frac{\overline{e}}{2}, B_3 = \frac{\overline{e}^2}{8} \tag{8}$$

If the chief orbit is near circular (i.e. $\overline{e}_{\mathcal{C}} \approx 0$) the explicit expressions for F_{11}, F_{12}, F_{21}, F_{22}, C_1 and C_2 can be written as (the subindex $\mathcal{C}$ is omitted for brevity):

$$\begin{aligned}
F_{11} &\approx -C_B\rho_0\sqrt{\frac{\mu}{\overline{a}}}I_0(0) \\
F_{12} &\approx -2C_B\rho_0\sqrt{\mu\overline{a}}\left[-\beta\overline{a}I_0(0)+(\beta\overline{a}+2)I_1(0)\right] \\
F_{21} &\approx C_B\rho_0\sqrt{\frac{\mu}{\overline{a}^3}}I_1(0) \\
F_{22} &\approx -2C_B\rho_0\sqrt{\frac{\mu}{\overline{a}}}\left[\left(\frac{1}{2}+\frac{1}{2}\beta\overline{a}\right)I_0(0)-\beta\overline{a}I_1(0)+\left(\frac{1}{2}+\frac{1}{2}\beta\overline{a}\right)I_2(0)\right] \\
C_1 &\approx -\overline{a}^2\frac{C_D}{m}\overline{n}\rho_0 I_0(0) \\
C_2 &\approx -\frac{C_D}{m}\overline{n}\rho_0\overline{p}I_1(0)
\end{aligned} \tag{9}$$

From Eq. (6) it can be calculated that $I_0(0)=1$, $I_1(0)=I_2(0)=0$. Thus, the linear time-varying dynamics for $\overline{e}_{\mathrm{c}} \approx 0$ are:

$$\begin{bmatrix}\Delta\dot{\overline{a}}\\ \Delta\dot{\overline{e}}\end{bmatrix} \approx \begin{bmatrix}-C_B\rho_0\sqrt{\frac{\mu}{\overline{a}}} & 2C_B\rho_0\sqrt{\mu\overline{a}}\beta\overline{a} \\ 0 & -2C_B\rho_0\sqrt{\frac{\mu}{\overline{a}}}\left(\frac{1}{2}+\frac{1}{2}\beta\overline{a}\right)\end{bmatrix}\begin{bmatrix}\Delta\overline{a}\\ \Delta\overline{e}\end{bmatrix} + \begin{bmatrix}-\overline{a}^2\frac{C_D}{m}\overline{n}\rho_0 \\ 0\end{bmatrix}\Delta S \tag{10}$$

Eq. (10) shows that for near-circular orbits $\Delta\dot{\overline{e}}$ remains unaffected by ΔS and $\Delta\overline{a}$. Thus, the differential mean eccentricity is uncontrollable in near-circular orbits.

3.2. Matching the Drag-Related Variation of the Semimajor Axis

It is well-known that the differential semimajor axis is the dominant factor affecting the inter-satellite distance, since different mean motions lead to secular growth of separation. Therefore, a cross-sectional area controller that matches the (osculating) drag-related semimajor axis variation of the modules will be designed. This matching is expected to significantly reduce the relative satellite drift. Other controllers, in which the differential cross-sectional area is modified as a function of, e.g., the along-track separation, may also considered.

The basic idea is that the cross-sectional area of the module with the larger semimajor axis is maximized, and the cross-sectional area of the other module is minimized. This idea is expected to be more efficient for low eccentricities, i.e. circular and near-circular orbits, and may not be effective for high eccentricities, where the difference in the semimajor axes does not uniquely determine which of the modules is higher.

It is reasonable to distinguish between two different effects in the temporal variation of the semimajor axis of each module. The first is short-periodic oscillations due to J_2 and the other gravitational harmonics, and the second is a secular variation due to the drag effect. The main concern is the secular variation; thus, the aforementioned control law will not use the osculating Δa of the modules. Instead, the secular difference in the semimajor axis caused by the drag only, defined by $\Delta a_{drag} \triangleq a_{\mathcal{D},drag} - a_{\mathcal{C},drag}$, will be used for feedback. This will also eliminate chattering related to the high-frequency content coming from the gravitational harmonics.

An important point is how to switch between the maximal and minimal cross-sectional areas of every module, when needed. In order to prevent discontinuities in the control, a sigmoid function of the form $\tanh\left(\Delta a_{drag}/\epsilon\right)$ is used, where ϵ is a small positive constant. This yields the following DD-based control law:

$$\begin{cases} \text{if } \Delta a_{drag} > 0 \Rightarrow \begin{cases} S_{\mathcal{D}} = S_{\mathcal{D},ref} + \tanh\left(\dfrac{\Delta a_{drag}}{\epsilon}\right)\left(S_{\mathcal{D},max} - S_{\mathcal{D},ref}\right) \\ S_{\mathcal{C}} = S_{\mathcal{C},ref} - \tanh\left(\dfrac{\Delta a_{drag}}{\epsilon}\right)\left(S_{\mathcal{C},ref} - S_{\mathcal{C},min}\right) \end{cases} \\ \text{if } \Delta a_{drag} < 0 \Rightarrow \begin{cases} S_{\mathcal{D}} = S_{\mathcal{D},ref} + \tanh\left(\dfrac{\Delta a_{drag}}{\epsilon}\right)\left(S_{\mathcal{D},ref} - S_{\mathcal{D},min}\right) \\ S_{\mathcal{C}} = S_{\mathcal{C},ref} - \tanh\left(\dfrac{\Delta a_{drag}}{\epsilon}\right)\left(S_{\mathcal{C},max} - S_{\mathcal{C},ref}\right) \end{cases} \end{cases} \tag{11}$$

In Eq. (11), $S_{\mathcal{D},ref}$ and $S_{\mathcal{C},ref}$ denote the reference areas, i.e. the cross-sectional areas desired for modules $\mathcal{D}$ and $\mathcal{C}$ when $\Delta a_{drag} = 0$, respectively. These reference areas must satisfy $S_{\mathcal{D},min} \le S_{\mathcal{D},ref} \le S_{\mathcal{D},max}$, $S_{\mathcal{C},min} \le S_{\mathcal{C},ref} \le S_{\mathcal{C},max}$.

3.3. Timing Considerations

Timing is an important consideration when performing DD maneuvers based on controller (11). The timing in which the DD controller is switched on will determine the evolution of the inter-satellite distance: If the controller is switched on when the relative distance is decreasing, then the relative distance growth can be negated, resulting in small relative distances among the satellites. On the other hand, if the controller is switched on when the distance is increasing, the drift will be arrested, but at a point in which the distance could already be prohibitively large.
Practically, it means that controller (11) should be activated at some $t = t_{start}$, where, in general, $t_{start} \neq t_0$. The value of t_{start} depends upon the particular scenario and the transient time, i.e., the time when $\Delta a_{drag} \approx 0$, denoted by t_{end}. This means that the application of DD maneuvers in practical scenarios should be coupled to orbit determination and prediction.

4. Extension to Multiple Modules

4.1. Cyclic Strategy

In the cyclic strategy, the DD control of N>2 modules is transcribed into N separate two-module control problems. Practically, it means that the reference semimajor axis of each module is the semimajor axis of an adjacent module. Thus, module i will track the semimajor axis of module $i+1$ (for i = 1, 2, 3 .... N-1), and module N will track the semimajor axis of module 1. Although this control logic may look somewhat similar to the case of two modules, there is an important difference. Whereas for N=2 the control law (11) defines the cross-sectional areas of both modules, for N>2 the proposed cyclic implementation will define the cross-sectional area of a single module. Consequently, the required cross-sectional areas are determined as follows:

$$S_i = \begin{cases} S_{i,ref} + \tanh\left(\dfrac{a_{i,drag} - a_{j,drag}}{\epsilon}\right)\left(S_{i,max} - S_{i,ref}\right), & a_{i,drag} \geq a_{j,drag} \\ S_{i,ref} + \tanh\left(\dfrac{a_{i,drag} - a_{j,drag}}{\epsilon}\right)\left(S_{i,ref} - S_{i,min}\right), & a_{i,drag} < a_{j,drag} \end{cases} \qquad (12)$$

$$j = \begin{cases} i+1,\ i = 1,2,3....N-1 \\ 1,\ i = N \end{cases}$$

Ref [20] contains the Lyapunov stability proof of the cyclic strategy.

4.2. Optimal Strategy

As opposed to the cyclic strategy, the idea here is to find a common reference semimajor axis for all the modules, $\tilde{a}$, so that

$$S_i = \begin{cases} S_{i,ref} + \tanh\left(\dfrac{a_{i,drag} - \tilde{a}}{\epsilon}\right)\left(S_{i,max} - S_{i,ref}\right), & a_{i,drag} \geq \tilde{a} \\ S_{i,ref} + \tanh\left(\dfrac{a_{i,drag} - \tilde{a}}{\epsilon}\right)\left(S_{i,ref} - S_{i,min}\right), & a_{i,drag} < \tilde{a} \end{cases} \qquad (13)$$

The value of $\tilde{a}$ can be determined so that it minimizes a given cost functional; a possible cost functional is the maximal cross-sectional area variation (so that deviations from the reference cross-sectional area, determined by mission specifications, are minimized), i.e. $J(\tilde{a}) = \max_i |\Delta S_i(\tilde{a})|$, $\Delta S_i(\tilde{a}) \triangleq S_i(\tilde{a}) - S_{i,ref}$.

Since the drag acceleration can only reduce the semimajor axis, the common reference semimajor axis must be equal to or smaller than the semimajor axis of any module i. Consequently, a static constrained min-max optimization problem can be formulated as follows:

Find $\tilde{a}^\star$ so that $\tilde{a}^\star = \arg\min_{\tilde{a}} J(\tilde{a}) = \arg\min_{\tilde{a}} \max_i |\Delta S_i(\tilde{a})|$ subject to $\tilde{a}^\star - \min_i a_{i,drag} \leq 0$.

Ref [20] proves that the solution for the aforementioned static constrained optimization problem is $\tilde{a}^\star = \min_i a_{i,drag}$. Practically, this result means that all the modules should use the minimal semimajor axis as reference at any moment of time. An asymptotic stability proof for controller (13) is provided in Ref. [20], including analytic examination of the controller performance.

4.3. Comparison Between the Two Strategies

There are two main differences between the cyclic and optimal strategies. The first is the overall maneuver time. The total time until the final convergence, where all the semimajor axes are equal, is smaller for the cyclic strategy. Moreover, the time until equalization of the first two semimajor axes is smaller. The second different between the strategies is the control effort, or the cross-sectional area changes. The total change in the cross-sectional areas is smaller in the optimal strategy. This result is expected, since the cost functional for the optimization problem was defined as the maximal cross-sectional area change among all the modules. The optimal strategy ensures that at least one module will not maneuver at all, which is the module with the minimal semimajor axis. In general, the optimal strategy will never use the minimal cross-sectional area, and all the modules will use the maximal and the reference cross-sectional areas. Hence, the control effort will be smaller when using the optimal strategy.

5. Simulation

5.1. Case Study

The DD-based cluster flight algorithms discussed above will be implemented on-board the Space Autonomous Mission for Swarming and Geolocation with Nanosatellites (SAMSON) project, which is a cluster of three identical 6U Cubesats [21].
The maximum allowable inter-satellite distance between any pair in the SAMSON cluster is 250 km, and the minimum allowable distance is 100 m [21]. The mass of each satellite is m=6 kg, and $C_D = 2.4$. The maximal and minimal cross-sectional areas are $\mathrm{S}_{\max} = 0.2\ \mathrm{m}^2$ and $\mathrm{S}_{\min} = 0.03\ \mathrm{m}^2$, respectively. The relatively large variation of the cross-sectional area is due to the deployable solar panels, which can increase the cross-sectional area almost by an order of magnitude, thus allowing improved controllability for DD-based cluster flight. The perturbation models used in the simulation contain zonal harmonics up to J_8, atmospheric drag (including the atmosphere's velocity, which was neglected in the analytical developments), and solar radiation pressure.
The simulations were performed for 3 nanosatellites, each of which represents a module. Let $\boldsymbol{\alpha}(t) = \left[a(t), e(t), i(t), \Omega(t), \omega(t), f(t)\right]^T$. The respective initial orbital elements, as determined by the SAMSON orbital injection conditions [21], are:

$$\begin{aligned} \boldsymbol{\alpha}_1(0) &= \left[6978\ \mathrm{km}, 0.001, 51.5^\circ, 0^\circ, 0^\circ, 0^\circ\right] \\ \boldsymbol{\alpha}_2(0) &= \left[6977.9\ \mathrm{km}, 0.001,\ 51.49^\circ, -0.2^\circ, 0^\circ, -0.8^\circ\right] \\ \boldsymbol{\alpha}_3(0) &= \left[6977.8\ \mathrm{km}, 0.001, 51.48^\circ, -0.4^\circ, 0^\circ, -1.6^\circ\right] \end{aligned} \tag{13}$$

5.2. Cyclic Strategy

Figure 1 depicts the distance evolution among the modules, according to the cyclic strategy (12). The relevant time history of Δa_{drag} for the 3 modules and the cross-sectional areas are shown in Fig. 2.

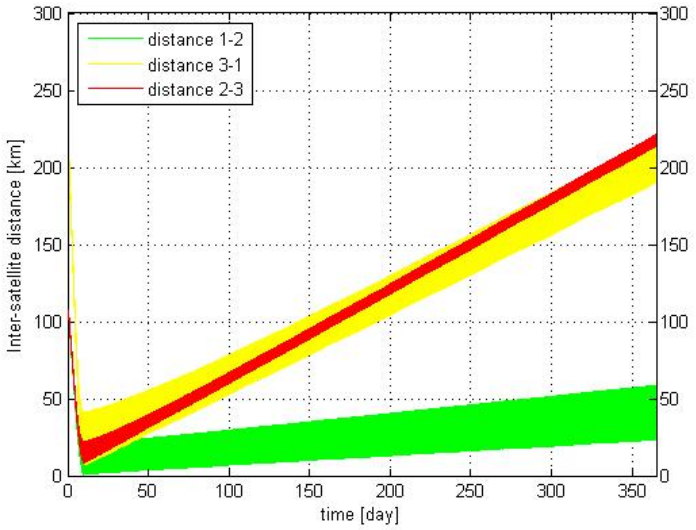

Figure 1. Cyclic strategy - inter-satellite distance evolution

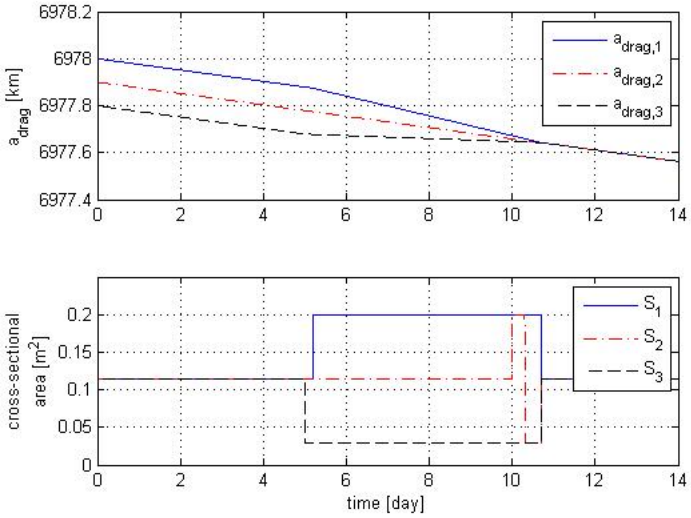

Figure 2. Cyclic strategy - $\Delta a_{drag}(t)$ and cross-sectional areas

The activation times of the DD controllers for this scenario are $t_{start,1} = 5.2$ days, $t_{start,2} = 10$ days and $t_{start,1} = 5$ days. The minimum distance between modules 1 and 2 is 0.236 km, at t=10 days. The rate of the inter-satellite distance growth between those modules after controller activation is 0.11 km/day, and the distance after 1 year is about 58.6 km.
The secular growth of the distance between module 2 and 3 after activation is 0.58 km/day, and the distance is about 221.4 km at the end of the simulation. The minimum distance between modules 2 and 3 is 8.4 km, at t=10.1 days.

The distance between modules 3 and 1 is bounded after activation by 220 km, for the 1-year simulation, with the minimum distance reaching 7.1 km at t=10.6 days. The secular growth of that distance after activation is about 0.54 km/day. Consequently, the maximum and minimum distance specification of SAMSON is satisfied.
The inter-satellite distances are reduced significantly by the DD controllers compared to uncontrolled motion: Without control, the maximal inter-satellite distance among the modules within the 1-year simulation is about 9540 km (which is the distance between modules 1 and 3 at t=365 days).

5.3. Optimal Strategy

Figure 3 depicts the inter-satellite distances, according to the optimal strategy (13). The relevant time histories of Δa_{drag} and the cross-sectional areas are shown in Fig. 4.

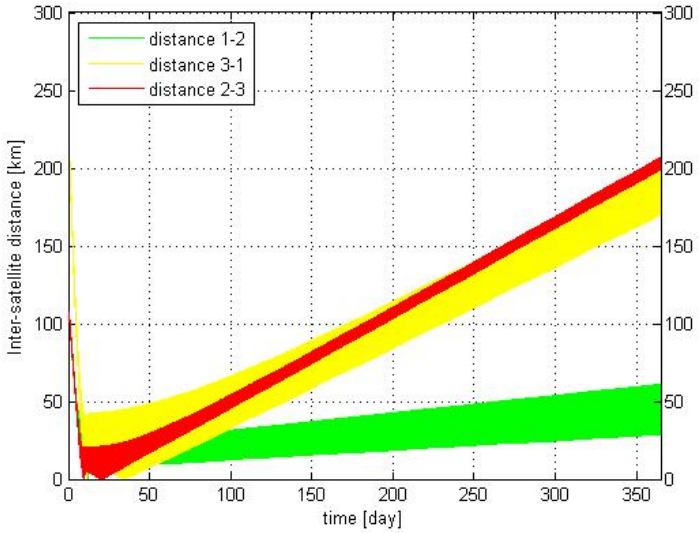

Figure 3. Optimal strategy - inter-satellite distance evolution

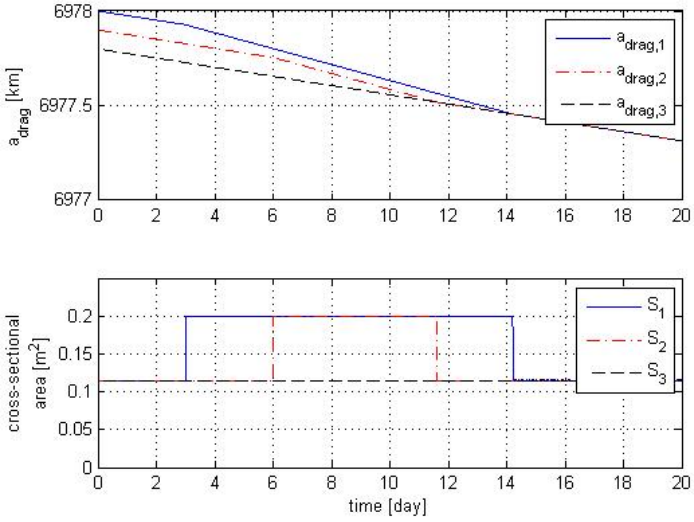

Figure 4. Optimal strategy - $\Delta a_{drag}(t)$ and cross-sectional areas

The activation times of the DD controllers for this scenario are $t_{start,1} = 3$ days, $t_{start,2} = 6$ days and $t_{start,3} = 5$ days.

The secular rate of change of the inter-satellite distance between modules 1 and 2 after activation is about 0.112 km/day, with the maximum distance reaching 61.1 km at the end of the 1-year simulation. The minimum distance between those modules after activation is 0.734 km, obtained at t=11.9 days.

The secular growth of the distance between modules 2 and 3 after activation is 0.584 km/day, with the minimum distance of 0.174 km at t=9.3 days. The upper bound on that distance after activation is 207 km, for the whole simulation.

The minimum distance between modules 3 and 1 is 0.297 km at t=36.3 days, while the maximum distance at the end of the simulation is 201.9 km. The secular rate of the distance is about 0.532 km/day, after activation. Here too, however, the SAMSON mission maximum and minimum distance specification is satisfied.

6. Conclusions

Using differential drag (DD) for mitigating the relative drift of a cluster of multiple low Earth-orbit satellites can be beneficial even for long-term missions. The orbital elements-based approach adopted herein captures the secular drag effect. Hence, the DD-based passive control of multiple satellite modules seems as a feasible means for keeping clusters of disaggregated satellites in orbit for long mission lifetimes, provided that there are relatively large differences between the minimum and maximum cross-sectional areas.

Acknowledgements

This work was supported by the European Research Council Starting Independent Researcher Grant # 278231: Flight Algorithms for Disaggregated Space Architectures (FADER).

References

[1] Schaub, H. and Alfriend, K. T., “Impulsive Feedback Control to Establish Specific Mean Orbit Elements of Spacecraft Formations,” Journal of Guidance, Control, and Dynamics, Vol. 24, No. 4, July-August 2001, pp. 739–745.

[2] D’Amico, S., Gill, E., and Montenbruck, O., “Relative Orbit Control Design for the PRISMA Formation Flying Mission,” Proceedings of the AIAA Guidance, Navigation and Control Conference, Vol. 1, 2006, pp. 474–492.

[3] Gill, E., D’Amico, S., and Montenbruck, O., “Autonomous Formation Flying for the PRISMA Mission,” Journal of Spacecraft and Rockets, Vol. 44, No. 3, May-June 2007, pp. 671–681.

[4] Mishne, D., “Formation Control of Satellites Subject to Drag Variations and J2 Perturbations,” Journal of Guidance, Control and Dynamics, Vol. 27, No. 4, July-August 2004, pp. 685–692.

[5] Beigelman, I. and Gurfil, P., “Optimal Fuel-Balanced Impulsive Formationkeeping for Perturbed Spacecraft Orbits,” Journal of Guidance, Control and Dynamics, Vol. 31, No. 5, September-October 2008, pp. 1266–1283.

[6] Lovell, T. A. and Tragesser, S. G., “Guidance for Relative Motion of Low Earth Orbit Spacecraft based on Relative Orbit Elements,” AIAA/AAS Astrodynamics Specialist Conference, Vol. 2, Providence, Rhode Island, 2004, pp. 644–658.

[7] Vaddi, S. S., Alfriend, K. T., Vadali, S. R., and Sengupta, P., “Formation Establishment and Reconfiguration Using Impulsive Control,” Journal of Guidance, Control and Dynamics, Vol. 28, No. 2, March-April 2005, pp. 262–268.

[8] Subbarao, K. and Welsh, S., “Nonlinear Control of Motion Synchronization for Satellite Proximity Operations,” Journal of Guidance, Control, and Dynamics, Vol. 31, No. 5, 2008, pp. 1284–1294.

[9] Gurfil, P., Idan, M., and Kasdin, N. J., “Neural Adaptive Control for Deep-Space Formation Flying,” Journal of Guidance, Control, and Dynamics, Vol. 26, No. 3, March April 2003, pp. 491–501.

[10] Leonard, C. L., Formationkeeping of Spacecraft via Differential Drag, Master’s thesis, Massachusetts Institute of Technology, 1986.

[11] Leonard, C. L., Hollister, W. M., and Bergmann, E. V., “Orbital Formationkeeping with Differential Drag,” Journal of Guidance, Vol. 12, No. 1, 1989, pp. 108–113.

[12] Blake, B. H., Satellite Formation Control using Atmospheric Drag, Master’s thesis, Air Force Institute of Technology, 2007.

[13] Kumar, B., Ng, A., Yoshihara, K., and De Ruiter, A., “Differential Drag as a Means of Spacecraft Formation Control,” IEEE Transactions on Aerospace and Electronic Systems, Vol. 47, No. 2, 2011, pp. 1125–1135.

[14] Kumar, B. and Ng, A., “A Bang-Bang Control Approach to Maneuver Spacecraft in a Formation with Differential Drag,” AIAA Guidance, Navigation and Control Conference and Exhibit, 2008, Paper AIAA 2008-6469.

[15] Bevilacqua, R. and Romano, M., “Rendezvous Maneuvers of Multiple Spacecraft Using Differential Drag Under J2Perturbation,” Journal of Guidance, Control, and Dynamics, Vol. 31, No. 6, pp. 1595–1607.

[16] Bevilacqua, R., Hall, J. S., and Romano, M., “Multiple Spacecraft Rendezvous Maneuvers by Differential Drag and Low Thrust Engines,” Celestial Mechanics and Dynamical Astronomy, Vol. 106, No. 1, 2010, pp. 69–88.

[17] Vallado, D. A., Fundamentals of Astrodynamics and Applications, Microcosm, Second Edition, 2001; Chapter 9, p. 592-593.

[18] Battin, R. H., An Introduction to the Mathematics and Methods of Astrodynamics, AIAA Education Series, 1987; Chapter 8, pp. 401-408; Chapter 10, pp. 495-508.

[19] King-Hele, D. G., “The Effect of the Earth’s Oblateness on the Orbit of a Near Satellite,” Proceedings of the Royal Society of London. Seires A, Mathematical and Physical Scinces, Vol. 247, No. 1248, September 1958, pp. 49–72.

[20] Ben-Yaacov, O. and Gurfil, P., “Long-term Cluster Flight of Multiple Satellites Using Differential Drag,” Journal of Guidance, Control and Dynamics, 2013, to appear.

[21] Gurfil, P., Herscovitz, J., and Pariente, M., “The SAMSON Project - Cluster Flight and Geolocation with Three Autonomous Nano-satellites,” 26th AIAA/USU Conference on Small Satellites, Salt Lake City, UT, USA, August 2012, Paper SSC12-VII-2.